



# Influence of the material manufacturing process on micromilling Ti6Al4V alloy

Maria Clara Coimbra Gonçalves<sup>1,2</sup> · Milla Caroline Gomes<sup>3,4</sup> · Rodrigo Lima Stoeterau<sup>1</sup> · Gilmar Ferreira Batalha<sup>1</sup> · Márcio Bacci da Silva<sup>3</sup>

Received: 23 February 2023 / Accepted: 23 August 2023 / Published online: 11 September 2023  
© The Author(s), under exclusive licence to Springer-Verlag London Ltd., part of Springer Nature 2023, corrected publication 2023

## Abstract

In order to obtain miniaturised products, additive manufacturing (AM) combined with micromachining presents a great potential on reducing manufacturing costs and material waste. The machinability of metals in general is well known for conventional machining processes. However, for micromachining processes, there are still gaps regarding the material's behaviour. Likewise, the machinability of materials obtained by additive manufacturing still needs to be investigated. In this context, the present work aims to compare the micromilling process of an additive manufactured Ti6Al4V alloy produced by laser powder bed fusion (LPBF) and a commercial wrought Ti6Al4V alloy. The samples were examined through scanning electron microscope (SEM), energy-dispersive x-ray spectroscopy (EDS), and Vickers hardness measurements. No statistical differences were obtained when comparing the machining forces, burr formation, and surface roughness when micromilling the AM and wrought alloys. It was observed that the minimum chip thickness was not achieved in the experiments with higher tool diameter and lower feed per tooth, which led to a different workload on each edge of the tool. Better surface roughness was obtained in the combination of higher cutting speed and lower tool diameter. The experiments with lower material removal rate led to higher burr formation. From these analyses, it is possible to better understand the machinability of the Ti6Al4V alloy produced by AM.

**Keywords** Micromilling · Additive manufacturing · Ti6Al4V alloy · Machining

## 1 Introduction

Micromilling is an important machining process that produces components with high dimensional and geometrical accuracy and good surface finishing for distinct applications. This process is applied across the aerospace, biomedical, electronics, and automotive industries, enabling the manufacturing of small and complex geometries using various materials [1, 2]. Therefore, these industries directly benefit from the development of this manufacturing processes, which continually establishes new and innovative applications over the years [3, 4].

In general, micromilling differs from the conventional milling process by the dimensions of the cutting tools used, as defined by Aramcharoen et al. [5] and Câmara et al. [6], who determine the diameter of microtools ranging from 1 to

1000  $\mu\text{m}$ . For Masuzawa [7], the term “micro” is related to quantities that vary from 1 to 999  $\mu\text{m}$ . Other researchers also define this process based on the values of the chip thickness used, Ng et al. [8] defined that the chip thickness varies from 10 nm to 2  $\mu\text{m}$ . Thus, it can be seen that there is no consensus regarding the definition of micromilling. This is due to the considerable scale reductions present in micromachining processes, which cause specific phenomena, explained by the size effect [9]. The size effect occurs when the section thickness becomes comparable to the radius of the cutting edge and the grains of the machined surface. Thus, the cutting thickness, the cutting edge radius and the grain size of the machined material have great influences on the cutting process [4].

Therefore, due to the scale effect, in micromachining the cutting edge radius cannot be neglected as in macromachining, since it can be comparable to the grain size of the machined material [10]. In this condition, the edge cutting round of the microtool will be able to remove material in just one grain. The cutting thickness is also comparable to the

✉ Maria Clara Coimbra Gonçalves  
mclara.coimbra@usp.br

Extended author information available on the last page of the article

tool's cutting edge radius [6]. For chip formation to occur in micromachining, it is necessary that the thickness of cut has a minimum value. If the thickness is less than the minimum, friction and ploughing phenomena may occur until the cutting thickness reaches the minimum value for chip formation [4].

Another common manufacturing process applied in industry is powder bed fusion (PBF) [11]. PBF is an additive manufacturing (AM) technique used to produce 3D parts with optimised topology using thermal energy provided by electron or laser beams that selectively melt and fuse the material in a powder bed [12]. Among the advantages of this process, its better use of raw material, waste reduction, and *near net shape* production of components can be highlighted [13, 14]. However, parts additively manufactured by PBF present high surface roughness, low dimensional and geometric accuracy, and high residual stresses [11]. For these reasons, post-processing techniques are required to achieve the dimensional and geometrical tolerances, surface quality and the desired mechanical properties of a part.

Currently, micromachining processes are being used as post-processing techniques for parts manufactured by AM. In this way, one part can be designed in its *near net shape* form, then machined to achieve its established surface roughness and dimensional tolerances [15]. In addition, the combination of micromachining processes with AM is cost-effective [16, 17] as it reduces the amount chips generated and minimises the use of cutting fluid, and therefore, contributes to a lower environmental impact than if compared to machining itself [1, 16, 17].

In the area of micromilling titanium alloys, Carou et al. [18] made a review classifying works regarding surface quality, cutting tools, lubrication systems, simulation and process monitoring and optimization. Biermann et al. [19] addressed the micromilling of complex shapes and its importance for medical applications. Willert et al. [20] stated that the hardness of titanium alloys is an important parameter that affects cutting force and surface finishing in micromachining. Lv et al. [21] concluded that the main wear mechanisms during micromilling titanium alloys are adhesion and abrasion, due to this material hardness, low thermal conductivity and reduced resistance in higher temperatures. In addition, Pratap et al. [22] stated that the interaction between tool and workpiece requires new studies due to the miniaturization of both parts.

Later, Balázs et al. [23] published an extensive review on the recent advances and future trends on micromilling. The authors concluded that the application of micromilling for producing 3D parts faces many challenges, such as: tool wear, that leads to inappropriate machined surfaces and tool breakage; burr formation, which is difficult to remove; unex-

pected vibration modes, that often leads to tool breakage. In addition they mentioned that this process is difficult to predict due to the size effect and difficulty to monitoring due to the relatively small forces and measures.

Even though many research ([18–22]) are found in the micromilling area, and the majority of them focus on micromilling titanium alloys (18.5% of the papers according to Balázs et al. [23]), only few research was found in micromilling additive manufacturing Ti6Al4V alloy grade 23 produced by PBF. In this area, Campos et al. [15] made a comparison on the machinability of commercial and AM workpieces, for this purpose, the cutting forces, surface roughness, burr formation analysis and microchips morphology were analysed. However, the variation of cutting speed was not analysed in their work, which has a major influence on the process mechanics, as a smaller cutting speed may lead to higher burr formation, which is undesirable in machining processes [24, 25]. In their work, the authors found that the cutting forces were lower for the AM sample and surface roughness behaviour was similar for the AM and commercial workpieces. Abeni et al. [26] also made a research comparing the micromachining of conventional and PBF samples by measuring the surface roughness and cutting force outcomes. The authors adopted cutting speed values from 30 to 50 m/min; however, the printing strategies adopted by the authors for the PBF process significantly differ from what was used in the present work. This can significantly change the micromilling results, as the consolidation process of the melted material changes. In their results, the authors found that the surface roughness of the samples was dependent on the sample fabrication technique, where samples manufactured through PBF presented better surface roughness [26]. As it can be noticed, the results vary from one work to another, which implies that more studies should be carried out in order to better understand the mechanics of cutting of the micromilling process.

In this perspective, this work aims to contribute to the investigation of the micromilling process outcomes for the Ti6Al4V alloy produced by LPBF. In that regard, the main objective of this work was to compare the forces, surface finishing and burr formation when micromilling a commercial wrought sample and an additive manufactured sample. Both samples were made of Ti6Al4V alloy grade 23, which is a material with lower interstitial elements widely applied in dentistry and medical industries [27]. In the present work, the printing strategy adopted an interlayer rotation of 67° in order to achieve optimum spacing between the angles during the AM process [28]. Thereby, for the set of parameters applied, the main differences on the micromilling process results for the AM and commercial alloy are described.

## 2 Materials and methods

### 2.1 Samples manufacturing and characterisation

Two different types of samples were used for the experiments: commercial and additive manufactured ones. The commercial sample was a wrought Ti6Al4V alloy, and the AM samples were made from Ti6Al4V powder with an average particle size of  $43.5 \mu\text{m}$  through the Laser Powder Bed Fusion (LPBF) process. The AM samples were manufactured in a 3D-printer OMNISINT-160 (Fig. 1a), using a Ytterbium fibre laser in an Argon atmosphere. The AM strategy applied was of a sequential sweeping band of  $5 \text{ mm}$  and an interlayer rotation of  $67^\circ$  (Fig. 1b). No heat treatment was performed in the AM sample before the micromilling experiments.

The samples microstructures were analysed with a scanning electron microscope (SEM) after a Keller's reagent etching, and an EDS analysis was performed in order to check their chemical composition [29]. Figure 2a and c show the samples backscattered electron's image ( $\times 2000$  augmentation) and its EDS analyses for the commercial sample, and Fig. 2b and d show the same analyses for the AM samples. The samples characteristics (hardness, dimensions and microstructure) are summarised in Table 1.

The bimodal microstructure highlighted on the commercial sample presents its equiaxed  $\alpha$ -phase in darker grey and a transformed  $\beta$ -phase in lighter grey (Fig. 2a). This microstructure results in a sample with good mechanical strength and good ductility due to the reduction of the lamellar matrix [30]. The  $\alpha$  grain sizes are about  $15\text{--}20 \mu\text{m}$  and its chemical composition is shown in the EDS analysis (Fig. 2c). The hardness of the commercial sample, averaged out of 10 measurements, was  $332.3 \pm 4.54 \text{ HV}50$ .

The AM strategies applied for manufacturing the samples were previously defined in the work of [31] and aimed to achieve mechanical properties results as close as possible to the commercial manufactured alloy, as proposed in the ASTM F3001 standard [32]. The AM parameters used are shown in Table 2. The powder used for manufacturing the sample was a Ti6Al4V grade 23 ELI. From Fig. 2b it is possible to observe the formation of  $\alpha'$ -martensite in the AM

alloy, which is a result of a diffusionless transformation due to rapid cooling of the LPBF process. These thin martensites laths with tight spacing between them prevents dislocations motion, what leads to a material with low ductility and high strength [33]. The mean porosity of the AM samples was estimated by SEM images around  $0.31 \pm 0.06 \%$ . The hardness of the AM samples, averaged out of 10 measurements, was  $369.1 \pm 5.36 \text{ HV}30$ .

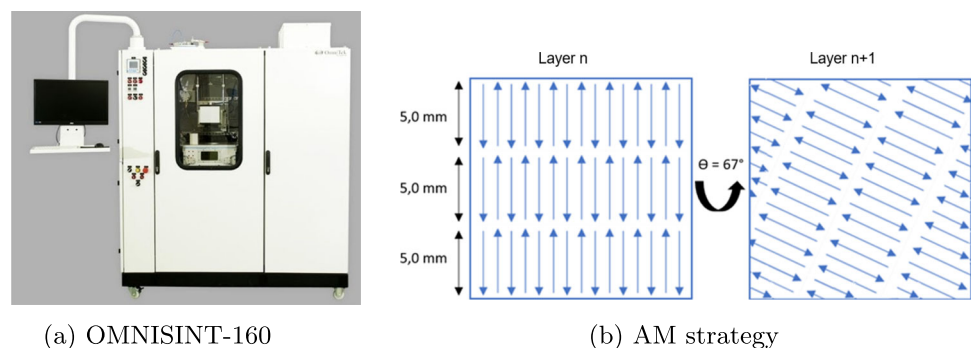
### 2.2 Micromilling experiments and force measurements

The micromilling tests were performed using a 3 axis CNC Mini-mill/GX by Minitech Machinery Corporation, with a maximum feed rate of  $1000 \text{ mm/min}$ , and maximum spindle speed of  $60,000 \text{ rpm}$  (Fig. 3a). The positioning error associated with the machine is  $0.1 \mu\text{m}$  and it is controlled through a Mach3Mill CNC software.

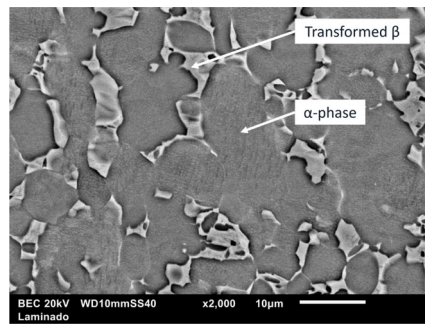
The experiments consisted in manufacturing microchannels on both samples, commercial and additive manufactured. The microchannel length was  $12$  and  $20 \text{ mm}$  for the AM and conventional samples, respectively. For each channel manufactured, the forces in X and Y directions were acquired. The feed force is in Y direction. For the acquisition of these forces a Kistler MiniDyn model 9256C2 was used together with a Kistler conditioner model 5019, an acquisition board from National Instruments model NI USB-6551 and a computer with the LabView Signal Express software. An illustration of the force acquisition system is presented in Fig. 3b. The signals were obtained with an acquisition rate of  $100 \text{ kHz}$  and a Savitzky-Golay filter with a cubic polynomial and a window size of 51 points was used for smoothing the noise on the data. Also, during the experiments, the room temperature was kept at  $20^\circ \text{C}$  to avoid linear thermal expansion changes.

Table 3 presents the parameters used for each test. The cutting conditions were defined based on previous experiments carried out at the LEPU-UFU laboratory and based on preliminary tests carried out at USP-SP. The cutting edge radius of each microtool was analysed to determine the feed per tooth to be used, and the goal was to investigate the cut with

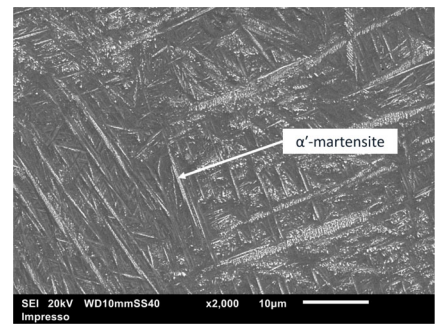
**Fig. 1** AM printer and strategy applied



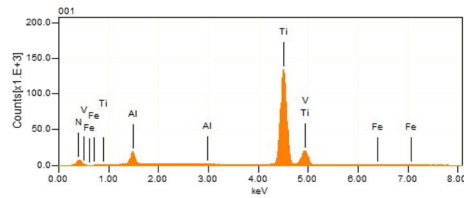
**Fig. 2** SEM analyses for the commercial and AM samples



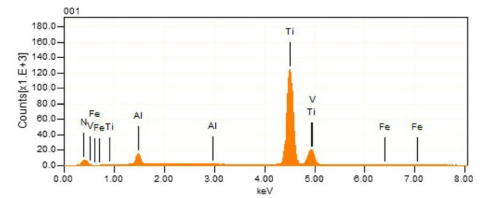
(a) Commercial sample microstructure



(b) Additive manufactured sample microstructure



(c) EDS analysis for the commercial sample



(d) EDS analysis for the additive manufactured sample

**Table 1** Samples characteristics

Sample	Hardness	Dimensions	Microstructure
Commercial sample	332.3 ± 4.54 HV50	20 mm wide and 60 mm long	bimodal
AM samples	369.1 ± 5.36 HV30	12 mm wide and 12 mm long	α'-martensite

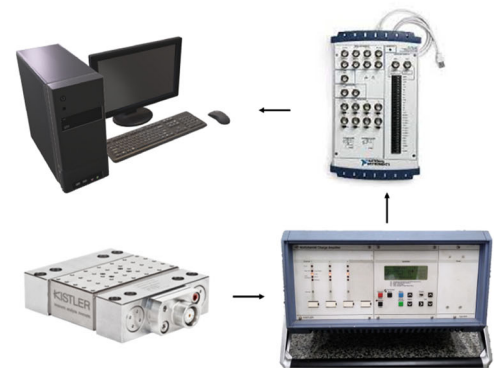
**Table 2** AM process parameters

Laser power [W]	Scanning speed [mm/s]	Layer thickness [μm]	Laser spot diameter [μm]
155	950	30	70

**Fig. 3** Experimental setup



(a) CNC Mini-mill/GX

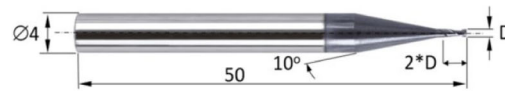


(b) Force data acquisition system

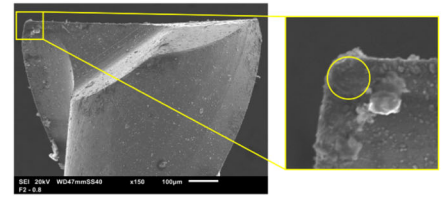
**Table 3** Micromilling process parameters

Workpiece	Tool diameter [mm]	Cutting speed [m/min]	Feed [μm/tooth]
AM	0.5 & 0.8	40 & 60	1, 1.5 & 2
Commercial	0.5 & 0.8	40 & 60	1, 1.5 & 2

Fig. 4 Micromills



(a) Micromill geometry



(b) Tool nose radius

the dominant presence of ploughing and without its presence. Therefore, the edge radius was estimated from its measurement on the secondary clearance surface. The value obtained for the largest microtool diameter was  $1.5 \mu\text{m}$  and for the one with the smallest diameter,  $1.3 \mu\text{m}$ . Therefore, feed values per tooth of  $(1\text{--}1.5\text{--}2.0) \mu\text{m/tooth}$  were selected. Since  $1 \mu\text{m/tooth}$  is smaller than the edge radius, therefore ploughing will be dominant. However, for the highest feed ( $2.0 \mu\text{m/tooth}$ ) the ploughing effect will not be dominant, and an intermediate condition was also selected ( $1.5 \mu\text{m/tooth}$ ). In addition, it was decided to vary the diameter of the microtool to observe its influence on the micromilling process. The depth of cut was set constant at  $25 \mu\text{m}$ .

For the tests, a total of 12 tungsten carbide TiAlN coated micro-end mills with two cutting edges were used. The tools present an helix angle of  $35^\circ$  and its geometry is illustrated in Fig. 4a. The two different tool diameters ( $D$ ) adopted for the experiments were:  $0.5 \text{ mm}$  and  $0.8 \text{ mm}$ . To check the tool integrity before the experiments, they were observed in SEM microscope. From SEM images, the tool nose radius was determined using the ImageJ software. For  $0.5 \text{ mm}$  tools the nose radius was approximately  $1 \mu\text{m}$  and for  $0.8 \text{ mm}$ ,  $5 \mu\text{m}$  (Fig. 4b, x150 magnification). Furthermore, the integrity of the tools were periodically monitored in the microscope during the micromilling experiments to assure that no significant tool wear or tool damage were affecting the process.

### 2.3 Additional measurements

The surface roughness and burr formation of the micromilled channels were also measured. The surface roughness was evaluated in terms of surface texture field parameters using a non-contact Taylor Hobson 3D CCI profilometer. The analysed parameters were the arithmetic mean of the area ( $S_a$ ) and the root mean square height ( $S_q$ ). The skewness ( $S_{sk}$ ) and kurtosis ( $S_{ku}$ ) were also examined to respectively assess the height distribution on the surface and the peaks and valleys tip geometry. The surface roughness parameters were measured three times along each channel (around the beginning, middle, and end of the channel) and before these measurements, all samples went through ultrasonic cleaning.

For an estimative of top burr formation, SEM images of the channels for each condition were evaluated using the image-

processing software ImageJ. The SEM images were acquired in the middle of the channel as a standard procedure. Aiming to quantify the burr area from these figures, each image was separately scaled and converted into a binary image for making its analysis. This way, the burr stood highlighted and its pixel's percentage was estimated, allowing a comparison between the acquired images.

## 3 Results and discussion

### 3.1 Machining forces

Regarding the machining forces, both  $F_x$  and  $F_y$  were measured and analysed. First, an illustration of the raw data and how the Savitzky-Golay filter smooths the signal is shown in Fig. 5. Following the forces analyses procedure, Fig. 6 shows an example of the entire force signal and how it was zoomed for further analyses.

From the results, no significant changes between the AM and commercial alloys were observed, which is different from what was found by Abeni et al. [26] and Campos et al. [15] that also carried out a comparison between the machinability of the Ti6Al4V alloys manufactured conventionally and by additive manufacturing. Figures 7 and 8 present the  $F_x$  and  $F_y$  machining force data, respectively, zoomed around  $5 \text{ mm}$  of the channel length. From that, it can be observed that the results visually present the same behaviour for the same set of cutting parameters for the commercial and AM alloys, including its magnitude. For

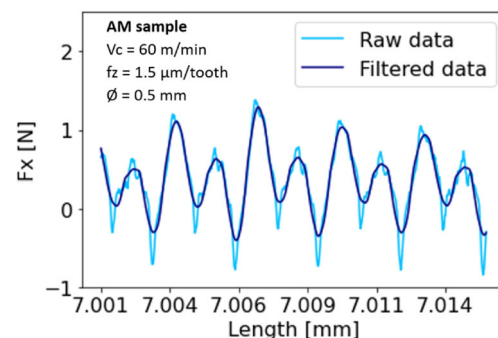


Fig. 5 Raw and filtered data comparison

Fig. 6 Forces data zooming

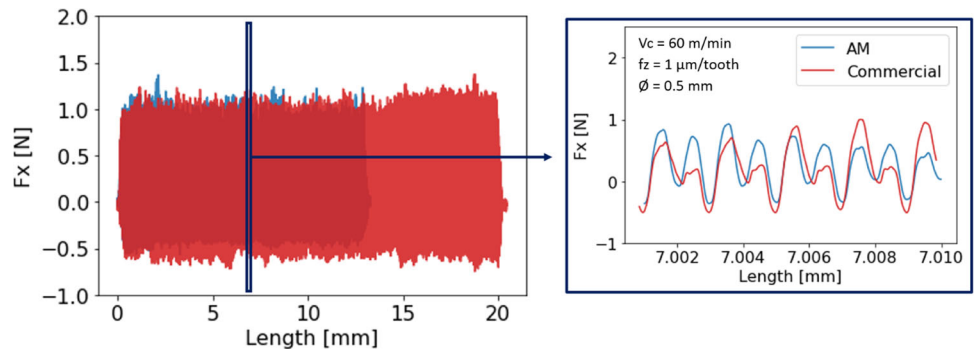
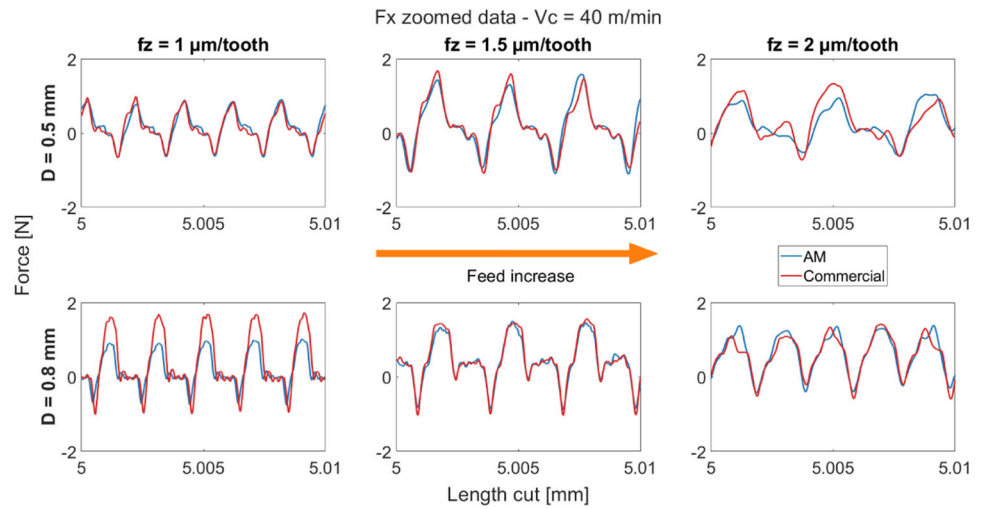
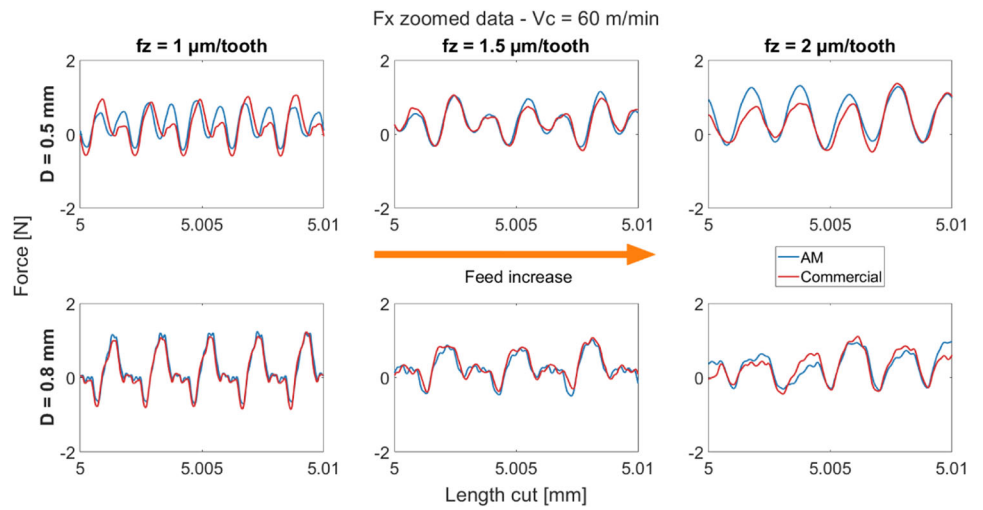


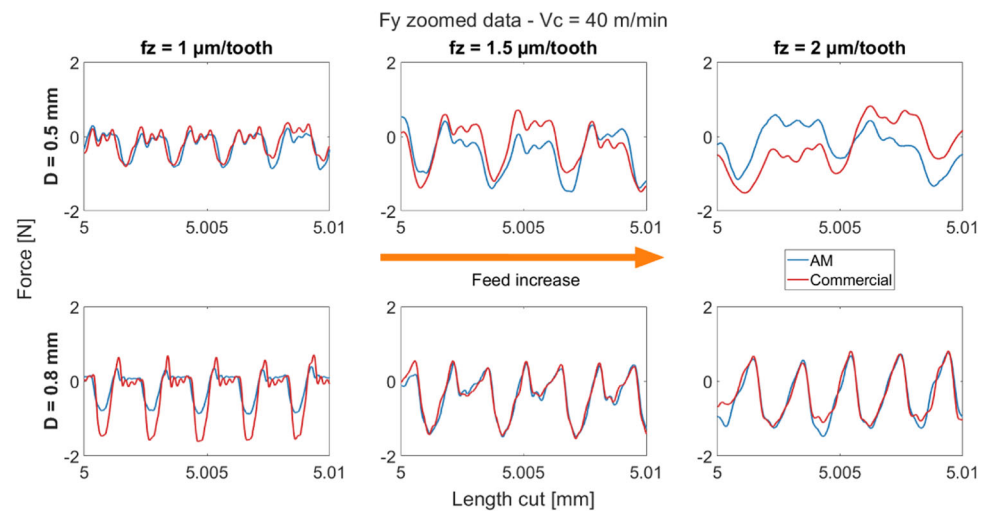
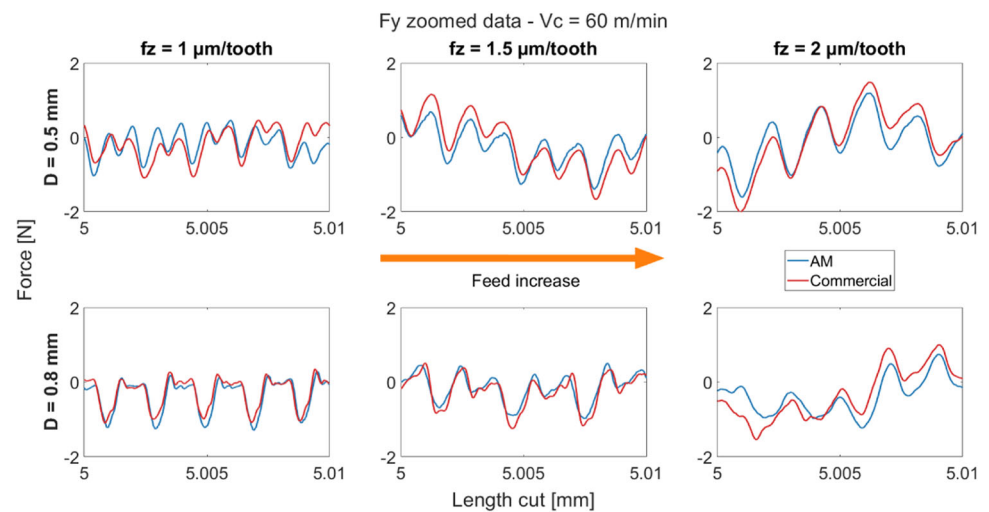
Fig. 7 Fx force results



(a)  $F_x$  force results for cutting speed of 40 m/min.



(b)  $F_x$  force results for cutting speed of 60 m/min.

Fig. 8  $F_y$  force results(a)  $F_y$  force results for cutting speed of 40 m/min.(b)  $F_y$  force results for cutting speed of 60 m/min.

that reason, correlation analyses were made, estimating the Pearson coefficient, to measure the relationship between the material and the machining forces results. The Pearson coefficients obtained were 0.063 and 0.018 for  $F_x$  and  $F_y$  forces, respectively. Since these coefficients are close to zero, it indicates that there is no statistical relation between the material being cut and the machining forces results. This is due to the AM strategy adopted that aimed to produce an alloy with mechanical properties similar to the commercial alloy, even though they present different microstructures.

Regarding the force's magnitude,  $F_x$  and  $F_y$  are in the same range (varying up to 2 N). However, the  $F_x$  results seemed more reliable, as the action of each tooth is clearer in these results. It was also observed that there was a correlation between  $F_x$  and cutting speed. In most cases, when cutting speed increased, forces decreased, as it is usual in conventional milling process.

In this perspective, when analysing Fig. 7, it is possible to observe the contribution of each cutting edge of the tool on the  $F_x$  forces. In one rotation of the tool, the cutting edge comes into contact with the workpiece causing an initial crushing of the material, and gradually, the uncut chip thickness increases until reaching its maximum value. After that, the peak force decays, as uncut chip thickness decreases. Then, the processes of plastic deformation, elastic recovery, chip formation and material removal start again on the second cutting edge. In this dynamic, as the chip load increases, the machining forces increases and vice-versa, what leads to the sinusoidal shape of the force curve.

It is possible to observe from Fig. 7 that asymmetric cut was occurring for some of the experiments. According to Picard et al. (2022) this is due to tool run-out [34] and it leads to one edge of the tool not effectively cutting the material. In this case, one tooth of the tool is crushing the material

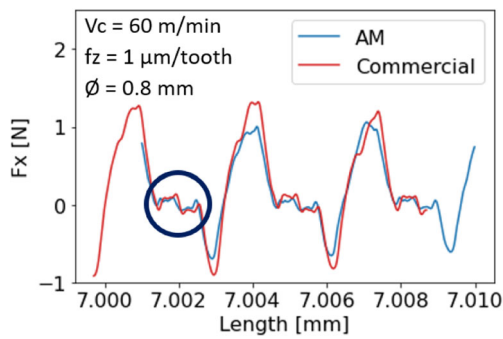


**Fig. 9** Forces results for lower feed rate and higher tool diameter with emphasis on one edge of the tool not effectively cutting the material

and elastically deforming it, leading to smaller machining forces results. Then, the most heavily loaded tooth will cut the amount of material it should originally cut plus the amount of material left by the other cutting edge, leading to the maximum uncut chip thickness twice the feed per tooth [34]. This behaviour (highlighted in Fig. 9) is also observed on normal scale process when the radial cutting depth is small on free cutting, when the axial cutting depth is smaller than the radius nose, or when the feed rate is too small on grooving milling.

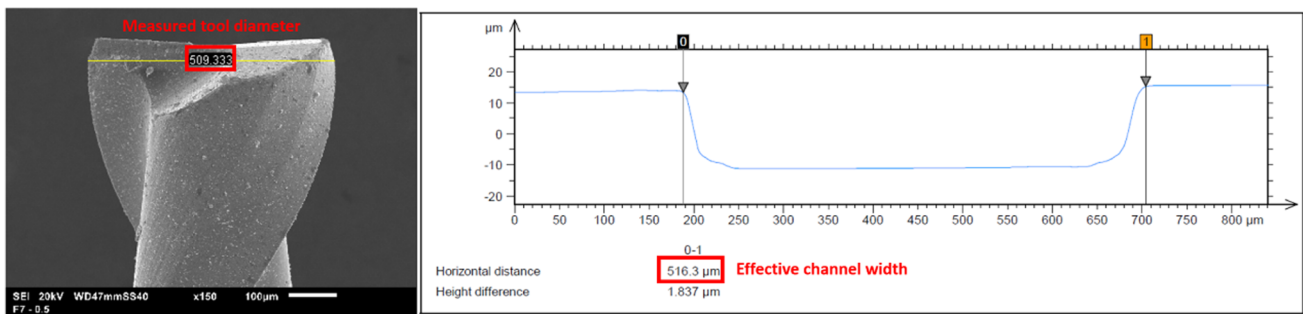
In order to estimate tool run-out, the channel width was measured and compared to the measured tool diameter (Fig. 10). From this analysis, it can be observed that tool

run-out was in the range found in literature [30, 35, 36], with a difference of less than 2% from the tool diameter and the effective channel width. This means that the precision of our channels is  $\pm 16 \mu\text{m}$  in the worst case and the chip thickness due to run-out is altered.

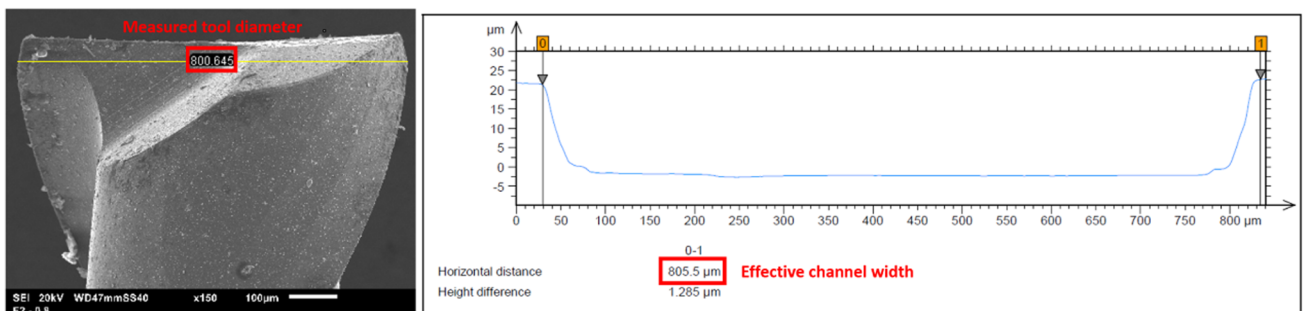
### 3.2 Surface roughness

From the surface roughness results, it could be observed that there is a statistical correlation between the cutting speed and the arithmetic mean of the area ( $S_a$ ) and the root mean square height ( $S_q$ ). The  $S_a$  results are graphically represented in Fig. 11 together with the 3D topographical representation of the highlighted points (lower feed per tooth). As can be seen, the surface roughness increases with lower speed, and the best surface roughness results were achieved with lower diameter tools. However, no correlation can be settled between feed per tooth and surface roughness values.

Indeed, the cutting speed affects the surface roughness because the material removal rate increases with the increase of cutting speed [37], what makes the surface smoother. Although, the relationship between the surface roughness and cutting speed is not analytical [38]. Wang et al. [39], for example, obtained higher surface roughness for higher speeds, as mentioned by the authors, this intriguing behaviour in their work was attributed to the occurrence of high-frequency vibrations of the system at higher speeds.



(a) Tool diameter and effective channel width for 0.5 mm diameter tool



(b) Tool diameter and effective channel width for 0.8 mm diameter tool

**Fig. 10** Tool run-out measurement for both tools



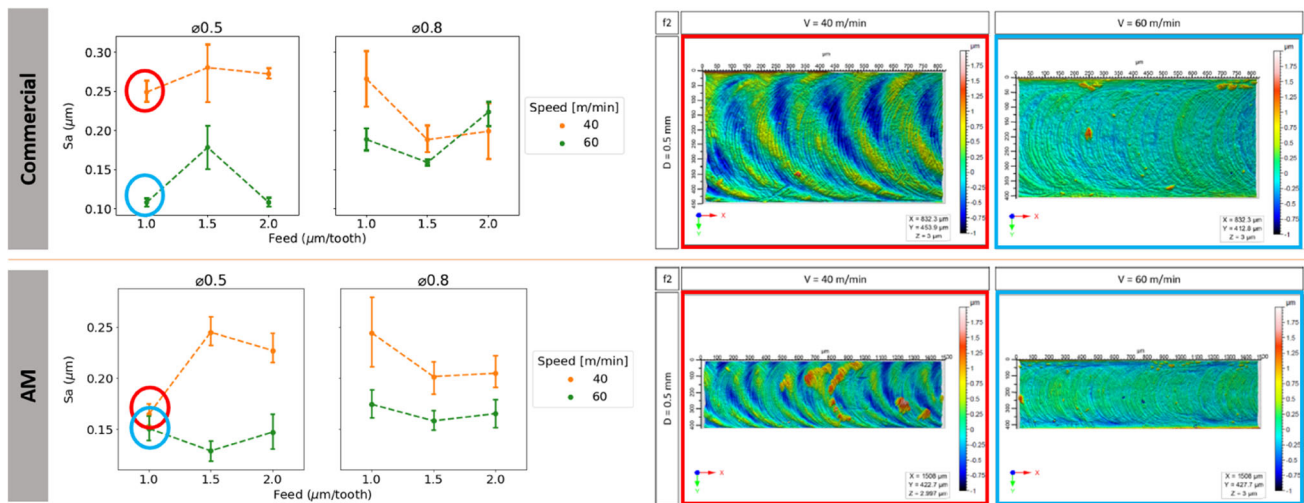


Fig. 11 Surface roughness results

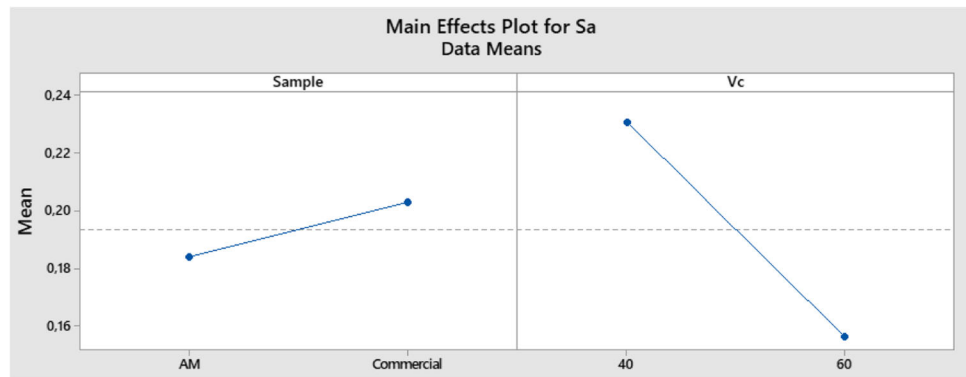
Other contributing factor to the final surface roughness is the tool diameter, as showed in literature [39, 40]. It was previously reported that the surface roughness increases with tool diameter due to the tool deformation that became bigger for smaller tool diameters [39]. Nevertheless, no clear relationship between tool diameter and surface roughness could be observed in the tests from the present work. However, better surface finishing was achieved for the lower tool diameter combined with higher cutting speed.

To check if these influences were statistically significant an analysis of variance with 5% significance level was made.

The results for the interaction between the independent variables and the  $S_a$  results are shown in Table 4. The performed ANOVA underlines that surface roughness is mainly affected by the cutting speed and the by the sample (commercial vs. AM). Also, the interactions of the sample with  $V_c$ , diameter with  $f_z$ , and  $V_c$ , the sample with diameter with  $f_z$  and  $V_c$ ,  $f_z$  with  $V_c$  with diameter and sample were statistically significant changing the  $S_a$  mean. For this reason, the main effect plot was made for the Sample and  $V_c$  parameters (Fig. 12), in which  $V_c$  was the most significant one. As it can be seen in Fig. 12, the  $S_a$  mean increased in the commercial sample, and

Table 4 ANOVA results

Source	DoF	Adj SS	Adj MS	F	P
Sample	1	0.004387	0.004387	9.14	0.006
Diameter	1	0.000441	0.000441	0.92	0.347
$f_z$	2	0.000262	0.000131	0.27	0.764
$V_c$	1	0.067058	0.067058	139.71	0.000
Sample*Diameter	1	0.000530	0.000530	1.10	0.304
Sample* $f_z$	2	0.000237	0.000118	0.25	0.783
Sample* $V_c$	1	0.002826	0.002826	5.89	0.023
Diameter* $f_z$	2	0.017680	0.008840	18.42	0.000
Diameter* $V_c$	1	0.017645	0.017645	36.76	0.000
$f_z$ * $V_c$	2	0.000120	0.000060	0.13	0.883
Sample*Diameter* $f_z$	2	0.005621	0.002810	5.86	0.008
Sample*Diameter* $V_c$	1	0.005558	0.005558	11.58	0.002
Sample* $f_z$ * $V_c$	2	0.003537	0.001768	3.68	0.040
Diameter* $f_z$ * $V_c$	2	0.005583	0.002792	5.82	0.009
Sample*Diameter* $f_z$ * $V_c$	2	0.000018	0.000009	0.02	0.982
Error	24	0.011519	0.000480		
Total	47	0.143021			

Fig. 12 Main effect plot for  $S_a$ 

the better surface roughness was achieved in higher speeds, due to the higher material removal rate.

Other observations about the surface could be made regarding its height distributions ( $S_{sk}$  parameter) and its peaks and valleys geometries ( $S_{ku}$  parameter). The results of  $S_{sk}$  were, for all experiments, greater than zero and the  $S_{ku}$  results, greater than three. From that, it can be concluded that for all experiments there was a peak predominance on the surface, since  $S_{sk}$  values were greater than zero. In addition, the  $S_{ku}$  results greater than three represents a large amplitude variation of the peaks and valleys. In other words, the surface presented extreme peaks and valleys results. Although, these results may have an influence of the chips left on the surface that were not removed with the ultrasonic cleaning.

### 3.3 Burr formation

Considering the top burr area results, Fig. 13 presents a comparison between the best and the worst cases achieved for AM and commercial alloys for both tool diameters. Higher

burr formation was observed for the smaller cutting speed, as the material removal rate is lower. Although, for the smaller tool diameter, the feed of  $1.5 \mu\text{m}/\text{tooth}$  lead to greater burr formation and worst surface roughness. For the greater tool diameter, higher burr formation was achieved when using feed of  $1 \mu\text{m}/\text{tooth}$  and lower speed.

In addition, there was a correlation between feed force ( $F_y$ ) and burr formation, which was more expressive for the smaller tool diameter. In this case, burr formation was higher for the experiments with higher  $F_y$  forces and the Pearson coefficient obtained for the correlation analysis of data was 0.6. This happens because for greater feed force ( $F_y$ ), higher stresses are being generated in the feed direction, what increases compression and causes the lateral deformation of material. Indeed, top burrs are Poisson-type burrs, that happens as a result of lateral deformation of material [41]. However, no clear relation between burr area and feed force could be established for the  $0.8 \text{ mm}$  tool diameter, since the correlation was weak. This behaviour should be related to the variation of tool cutting edge radius for different tool sizes. diameters.

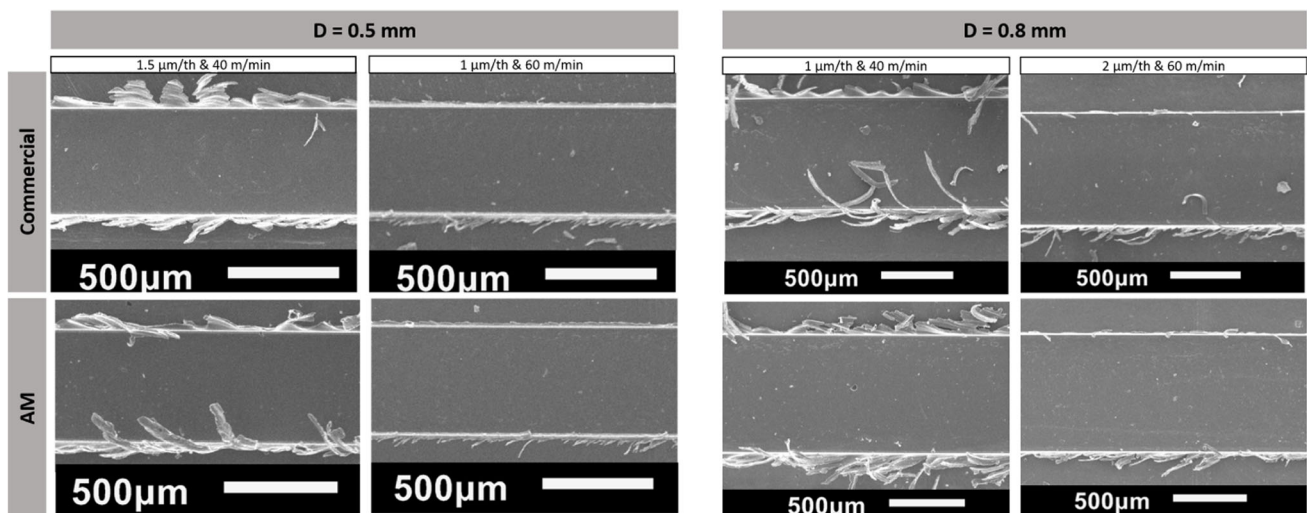


Fig. 13 Burr formation results

## 4 Conclusions

In this work, microchannels were fabricated in samples of titanium alloy Ti6Al4V wrought and manufactured by laser powder bed fusion, using the micromilling process. When analysing the machining forces, the surface roughness, and the burr formation, it was possible to conclude that:

- No statistically significant difference in the machinability of the commercial and the AM Ti6Al4V sample was observed during micromilling, for the set of parameters used. This is due to the AM strategy adopted that leads to similar mechanical strength of the AM and commercial samples;
- The forces magnitude during the micromilling process varied up to 2 N, for the adopted conditions;
- The analysis of the  $F_x$  force data revealed an asymmetric cutting phenomenon caused by tool run-out, which resulted in uneven chip load distribution across the tool edges;
- Regarding the surface roughness results, higher cutting speed led to better surface quality;
- The best surface roughness result was achieved with lower diameter tool and higher cutting speed, though, no relation could be settled between surface roughness and feed per tooth;
- For all experiments made, there was a predominance of extreme peaks on the surface, what is influenced by the chips left on the surface that were not removed by ultrasonic cleaning;
- Higher burr formation was observed on the small diameter tool experiments where higher  $F_y$  forces were measured. Consequently, surface quality on these experiments was harmed;
- For both tool diameters, the worst burr formation results were observed for the smaller cutting speed, as the material removal rate is lower in these cases.

Finally, from the analyses carried out, it was possible to observe that the results of machining force, surface roughness, and burr formation were similar for the wrought sample and the one manufactured by AM. In addition, for the set of parameters applied in this work, the microchannels with higher surface quality and less burr formation were achieved with the condition of a smaller tool diameter and higher cutting speed (60 m/min).

**Acknowledgements** The authors thank the National Council for Scientific and Technological Development (CNPq) for the financial support and Omnitek BR for providing the samples.

**Author contribution** All authors contributed to the study conception and design. Material preparation, data collection, and analysis were performed by Maria Clara Coimbra Goncalves and Milla Caroline Gomes.

The first draft of the manuscript was written by Maria Clara Coimbra Goncalves, edited by Milla Caroline Gomes and all authors commented on previous versions of the manuscript.

**Funding** This work was supported by the National Council for Scientific and Technological Development (CNPq), award number: 133231/2019-4

## Declarations

**Ethical approval** Not applicable.

**Consent to participation** Not applicable.

**Consent for publication** Not applicable.

**Competing interest** The authors declare no competing interests.

## References

1. Gomes MC, dos Santos AG, de Oliveira D, Figueiredo GV, Ribeiro KSB, Los Rios D, Hung W (2021) Micro-machining of additively manufactured metals: a review. *Int J Adv Manuf Technol* 1–20. <https://doi.org/10.1007/s00170-021-08112-0>
2. Kuram E, Ozcelik B (2015) Optimization of machining parameters during micro-milling of Ti6Al4V titanium alloy and Inconel 718 materials using Taguchi method. *J Eng Manuf* 231(2):228–242. <https://doi.org/10.1177/0954405415572662>
3. O'Toole L, Kang C-W, Fang F-Z. (2020) Precision micro-milling process: state of the art. *Ad Manuf* 9. <https://doi.org/10.1007/s40436-020-00323-0>
4. Cheng K, Huo D (2013) *Micro-cutting: fundamentals and applications*, 1st (edn). John Wiley, India. 978-0-470-97287-8
5. Aramcharoen A, Mativenga PT, Yang S, Cooke KE, Teer DG (2008) Evaluation and selection of hard coatings for micro milling of hardened tool steel. *Int J Mach Tools Manuf* 48:1578–1584
6. Câmara MA, Rubio JC, Abrão AM, Davim JP (2012) State of the art on micromilling of materials, a review. *J Mater Sci Technol* 28(8):673–685. [https://doi.org/10.1016/S1005-0302\(12\)60115-7](https://doi.org/10.1016/S1005-0302(12)60115-7)
7. Masuzawa T (2000) State of the art of micromachining. *CIRP Annals - Manuf Technol* 49:473–488. [https://doi.org/10.1016/S0007-8506\(07\)63451-9](https://doi.org/10.1016/S0007-8506(07)63451-9)
8. Ng CK, Melkote SN, Rahman M, Kumar AS (2006) Experimental study of micro- and nano-scale cutting of aluminum 7075–T6. *Int J Mach Tools & Manufacture* 46:929–936
9. Simoneau A, Ng E, Elbestawi MA (2006) Chip formation during microscale cutting of a medium carbon steel. *Int J Mach Tools Manuf Des Res Appl* 46(5):467–481
10. Sun Q, Cheng X, Liu Y, Yang X, Li Y (2017) Modeling and simulation for micromilling mechanisms. *Precis Eng* 174:402–407
11. Vafadar A, Guzzomi F, Rassau A, Hayward K (2021) Advances in metal additive manufacturing: a review of common processes, Industrial Applications, and Current Challenges. *Appl Sci*. <https://doi.org/10.3390/app11031213>
12. Ransikarbum K, Pitakaso R, Kim N (2020) A decision-support model for additive manufacturing scheduling using an integrative analytic hierarchy process and multi-objective optimization. *Appl Sci*. <https://doi.org/10.3390/app10155159>
13. Uhlmann E, Kersting R, Klein TB, Cruz MF, Borille AV (2015) Additive manufacturing of titanium alloy for aircraft components. *Procedia CIRP* 35:55–60. <https://doi.org/10.1016/j.procir.2015.08.061>

14. Chen LY, Huang JC, Lin CH, Pan CT, Chen SY, Yang TL, Lin DY, Lin HK, Jang JSC (2017) Anisotropic response of Ti-6Al-4V alloy fabricated by 3D printing selective laser melting. *Mater Sci Eng A* 682:389–395. <https://doi.org/10.1016/j.msea.2016.11.061>
15. de Oliveiras Campos F, Araujo AC, Munhoz ALJ, Kapoor SG (2020) The influence of additive manufacturing on the micromilling machinability of Ti6Al4V: a comparison of SLM and commercial workpieces. *J Manuf Process* 60:299–307. <https://doi.org/10.1016/j.jmapro.2020.10.006>
16. Ålgårdh J, Ströndl A, Karlsson S, Farre S, Joshi S, Andersson J, Ågren J (2017) State-of-the-art for additive manufacturing of metals. *Metalliska Mater*
17. Serres N, Tidu D, Sankare S, Hlawka F (2011) Environmental comparison of MESO-CLAD® process and conventional machining implementing life cycle assessment. *J Clean Prod* 19. <https://doi.org/10.1016/j.jclepro.2010.12.010>
18. Carou D, Rubio EM, Herrera J, Lauro CH, Davim JP (2017) Latest advances in the micromilling of titanium alloys: a review. *Procedia Manuf- Manuf Eng Soc Int Conf* 13:275–282. <https://doi.org/10.1016/j.promfg.2017.09.071>
19. Biermann D, Kahleiss F, Krebs E, Upmeier T (2011) A study on micro-machining technology for the machining of NiTi: five-axis micro-milling and micro deep-hole drilling. *J Mater Eng Perform* 20:745–751. <https://doi.org/10.1007/s11665-010-9796-9>
20. Willert M, Riemer O, Brinksmeier E (2016) Size effect in micro machining of steel depending on the material state. *Procedia CIRP* 46:193–196. <https://doi.org/10.1016/j.procir.2016.03.187>
21. Lv D, Xua J, Ding W, Fu Y, Yang C, Su H (2016) Tool wear in milling Ti40 burn-resistant titanium alloy using pneumatic mist jet impinging cooling. *J Mater Process Technol* 229:641–650. <https://doi.org/10.1016/j.jmatprotec.2015.10.020>
22. Pratap T, Patra K, Dyakonov A (2016) Modeling cutting force in micro-milling of Ti-6Al-4V titanium alloy. *Procedia Eng* 129:134–139. <https://doi.org/10.1016/j.proeng.2015.12.021>
23. Balázs BZ, Geier N, Takács M, Davim JP (2021) A review on micro-milling: recent advances and future trends. *Int J Adv Manuf Technol* 122:655–684. <https://doi.org/10.1007/s00170-020-06445-w>
24. Yadav AK, Kumar M, Bajpai V, Singh NK, Singh RK (2017) FE modeling of burr size in high-speed micro-milling of Ti6Al4V. *Precision Eng.* <https://doi.org/10.1016/j.precisioneng.2017.02.017>
25. Rehman GU, Jaffery SHI, Khan M, Ali L, Khan A, Butt SI (2018) Analysis of burr formation in low speed micro-milling of titanium alloy (Ti-6Al-4V). *Mech Sci* 231–243. <https://doi.org/10.5194/ms-9-231-2018>
26. Abeni A, Ginestra PS, Attanasio A (2022) Comparison between micro machining of additively manufactured and conventionally formed samples of Ti6Al4V alloy. *Selected Topics in Manufacturing*, Springer Nature Switzerland pp 91–106. [https://doi.org/10.1007/978-3-030-82627-7\\_6](https://doi.org/10.1007/978-3-030-82627-7_6)
27. Shokrani A, Dhokia V, Newman ST (2016) Comparative investigation on using cryogenic machining in CNC milling of Ti-6Al-4V titanium alloy. *Mach Sci Technol* 20(3):475–494. <https://doi.org/10.1080/10910344.2016.1191953>
28. Pakkanen J (2018) Designing for additive manufacturing - product and process driven design for metals and polymers. PhD Thesis, Politecnico di Torino
29. Gonçalves MCC (2022) Experimental investigation on micromilling machining of Ti6Al4V titanium alloy additively manufactured by Selective Laser Melting (SLM). Master's dissertation, Polytechnic School of the University of São Paulo
30. Attanasio A, Gelfi M, Pola A, Ceretti E, Giardini C (2013) Influence of material microstructures in micromilling of Ti6Al4V alloy. *Materials* 6:4268–4283. <https://doi.org/10.3390/ma6094268>
31. Podestá CE (2018) Spherical titanium powders produced through induction plasma and consolidated by selective laser melting. Master's dissertation IPEN - Nuclear and Energy Research Institute
32. ASTM (2014) Standard specification for additive manufacturing titanium-6 aluminum-4 vanadium ELI (extra low interstitial) with powder bed fusion1. Technical Report F3001 - 14, ASTM
33. Yang J, Yu H, Yin J, Gao M, Wang Z, Zeng X (2016) Formation and control of martensite in Ti-6Al-4V alloy produced by selective laser melting. *Mater Des* 108:308–318. <https://doi.org/10.1016/j.matdes.2016.06.117>
34. Piquard R, Coz GL, Fontaine M, Thibaud S (2022) A model of micro-milling cutting forces based on micro-cutting experiments including tool eccentricity and deflection. *Matériaux Tech* 110. <https://doi.org/10.1051/mattech/2022042>
35. Singh KK, Kartik V, Singh R (2019) Stability modeling with dynamic run-out in high speed micromilling of Ti6Al4V. *Int J Mech Sci* 150. <https://doi.org/10.1016/j.ijmecsci.2018.11.001>
36. Zhang X, Pan X, Wang G, Zhou D (2018) Tool runout and single-edge cutting in micro-milling. *Int J Adv Manuf Technol* 96. <https://doi.org/10.1007/s00170-018-1620-y>
37. Chen X, Ma L, Li C, Cao X (2014) Experimental study and genetic algorithm-based optimization of cutting parameters in cutting engineering ceramics. *Int J Adv Manuf Technol* 74:807–817. <https://doi.org/10.1007/s00170-014-5979-0>
38. Araujo AC, Mougo AL, de Oliveira Campos F (2021) Machining for engineering: a course on cutting mechanics, 1st (edn)., p 332. E-papers, Brazil. ISBN: 9786587065045
39. Wang W, Kweon SH, Yang SH (2005) A study on roughness of the micro-end-milled surface produced by a miniaturized machine tool. *J Mater Process Technol* 702–708. <https://doi.org/10.1016/j.jmatprotec.2005.02.141>
40. Manso CS, Thom S, Uhlmann E, de Assis CLF, del Conte EG (2019) Tool wear modelling using micro tool diameter reduction for micro-end-milling of tool steel H13. *Int J Adv Manuf Technol* 105:2531–2542. <https://doi.org/10.1007/s00170-019-04575-4>
41. da Silva LC, da Mota PR, da Silva MB, Ezugwu EO, Machado ÁR, (2015) Study of burr behavior in face milling of PH 13–8 Mo stainless steel. *CIRP J Manuf Sci Technol* 8. <https://doi.org/10.1016/j.cirpj.2014.10.003>

**Publisher's Note** Springer Nature remains neutral with regard to jurisdictional claims in published maps and institutional affiliations.

Springer Nature or its licensor (e.g. a society or other partner) holds exclusive rights to this article under a publishing agreement with the author(s) or other rightsholder(s); author self-archiving of the accepted manuscript version of this article is solely governed by the terms of such publishing agreement and applicable law.

## Authors and Affiliations

Maria Clara Coimbra Gonçalves<sup>1,2</sup>  · Milla Caroline Gomes<sup>3,4</sup> · Rodrigo Lima Stoeterau<sup>1</sup> · Gilmar Ferreira Batalha<sup>1</sup> · Márcio Bacci da Silva<sup>3</sup>

Milla Caroline Gomes  
millagomes150@gmail.com

Rodrigo Lima Stoeterau  
rodrigo.stoeterau@usp.br

Gilmar Ferreira Batalha  
gfbatalha@usp.br

Márcio Bacci da Silva  
mbacci@ufu.br

<sup>1</sup> Polytechnic School of Engineering (Poli-USP), University of São Paulo, Av. Prof. Luciano Gualberto, Butantã 05508-010, SP, Brazil

<sup>2</sup> Mechanical Engineering Department, University of Sheffield, Mappin Street, Sheffield S1 3JD, UK

<sup>3</sup> Federal University of Uberlândia, Av. João Naves de Ávila, Santa Mônica 38408-100, MG, Brazil

<sup>4</sup> Mechanical Engineering Department, Universidade Estadual de Campinas, Campinas, Brazil